Purdue University
Purdue e-Pubs

Other Nanotechnology Publications | Birck Nanotechnology Center

8-1-2006

An energy-based model for electrowetting-induced droplet actuation

Vaibhav A. Bahadur
Purdue University, vbahadur@purdue.edu

Suresh Garimella
School of Mechanical Engineering, sureshg@purdue.edu

Follow this and additional works at: http://docs.lib.purdue.edu/nanodocs

Bahadur, Vaibhav A. and Garimella, Suresh, "An energy-based model for electrowetting-induced droplet actuation" (2006). *Other Nanotechnology Publications.* Paper 16.
http://docs.lib.purdue.edu/nanodocs/16

This document has been made available through Purdue e-Pubs, a service of the Purdue University Libraries. Please contact epubs@purdue.edu for additional information.

INSTITUTE OF PHYSICS PUBLISHING JOURNAL OF MICROMECHANICS AND MICROENGINEERING

J. Micromech. Microeng. **16** (2006) 1494–1503 doi:10.1088/0960-1317/16/8/009

An energy-based model for electrowetting-induced droplet actuation

V Bahadur and S V Garimella

School of Mechanical Engineering, Purdue University, West Lafayette, IN 47907-2088, USA

E-mail: sureshg@purdue.edu

Received 15 February 2006, in final form 23 May 2006
Published 16 June 2006
Online at stacks.iop.org/JMM/16/1494

Abstract
Electrowetting (EW) induced droplet motion has been explored in the past decade in view of its promising applications in the field of microfluidics. This paper demonstrates the potential of energy-based analyses for modeling the performance of EW-based fluid actuation systems. Analyses based on system energy minimization offer simplified modeling tools to predict the overall performance of EW systems while circumventing the need to model the numerous complexities in the system. An analytical model is developed to estimate the actuation force on a droplet moving between two electrodes. The origins and contributions of various components of the actuation force are analyzed. The effects of dielectric parameters, electrode layout, droplet geometry and shape are discussed with the objective of maximizing the actuation force. The actuation force model is combined with semi-analytical models for predicting the forces opposing droplet motion to develop a model that predicts transient EW-induced droplet motion. Parametric results are obtained to evaluate the importance of operating voltage, fluid properties and droplet geometry on droplet motion.

(Some figures in this article are in colour only in the electronic version)

1. Introduction

Control of fluid motion at the microscale by tailoring surface tension is attractive for a range of microfluidic applications such as lab-on-chip systems, biomedical devices and other MEMS-based fluidic devices. A scaling analysis reveals that surface tension becomes dominant over pressure and body forces as systems scale down to the sub-millimeter range, pointing to an important tool for microfluidic flow control. Moving mechanical parts, undesirable in microscale systems, are usually not required for surface tension-based control. A number of surface tension-based fluid handling techniques have been discussed in the literature, the most significant among which include electrowetting (EW) [1] (reduction of interfacial tension by the application of an electric field), thermocapillarity-driven pumping [2] (reduction of surface tension by temperature, leading to fluid motion), opto-electrowetting [3] based pumping (light-controlled surface tension-induced pumping) and vapor bubble-based pumping [4].

Electrowetting has been used to demonstrate droplet actuation [5–11] and other microfluidic operations such as the formation, mixing and splitting of droplets [12]. There has also been noteworthy progress in understanding the physics governing phenomena which influence EW systems, such as contact-angle saturation [13], role of the electric double layer [14] and dynamics of the three-phase line [15]. Contact-line friction and contact-angle hysteresis are among the phenomena which remain incompletely resolved and pose significant challenges to modeling EW-based fluid motion. Additionally, the use of empirical velocity profiles [8, 16] in a discrete droplet to estimate viscous stresses is an assumption which has yet to be validated. Such complexities and uncertainties have limited attempts at modeling surface tension-induced droplet motion. The most comprehensive model for predicting *steady-state* EW-induced droplet motion was proposed by Ren *et al* [17], who arrived at the EW actuation force by estimating the pressure gradient across the droplet using the Laplace [18] equation. All the forces opposing droplet motion were represented by semi-empirical models consisting of multiple fitting parameters, which were obtained from experimental results. Kuo *et al* [8] modeled the EW-induced pressure gradient in terms of the contact-angle modification resulting

 © 2006 IOP Publishing Ltd Printed in the UK

from the application of an EW voltage. Oprins *et al* [16] modeled the EW actuation force on a droplet by estimating the electrostatic energy resulting from its equilibrium shape, under the action of electrostatic and surface tension forces. This was used in a transient droplet flow model which estimated the forces opposing droplet motion in a semi-empirical manner. Mohseni and Dolatabadi [7] developed a volume-of-fluid-based model to predict transient and steady-state droplet motion, with the EW effects introduced in terms of modified contact angles per Lippman's [18] equation.

The primary objective of this paper is to present an energy-based model for estimating the EW actuation force acting on a droplet during its transition. The results obtained from this model are exactly similar to those obtained from an electromechanical model. This shows EW-induced droplet motion as an electromechanical phenomenon, as opposed to a contact-angle change-induced effect. The actuation force model is purely analytical in nature and facilitates a deeper understanding of the physics governing EW actuation. The influence of actuation voltage, electrode and droplet geometries and dielectric parameters on the actuation force can be clearly understood using this model. The second objective of the paper is to combine the actuation force model with available semi-empirical models for predicting forces opposing droplet motion, to develop a means to predict transient EW droplet motion. The present work analyzes the suitability of these models for predicting droplet motion.

2. Energy-based modeling of electrowetting systems

The traditional concept of EWOD (electrowetting on dielectric) is founded on the premise of a reduction in dielectric–liquid interfacial energy by the application of a voltage between a conducting droplet and an underlying dielectric layer. In a recent paper, Jones [19] described electrowetting as an electromechanical phenomenon; however, the traditional interpretation of EW is used to develop the modeling framework in the present work and gives the same results as those obtained from a purely electromechanical model. To actuate droplets, the interfacial energy at one end of the droplet is reduced by applying a voltage to an electrode at that end of the droplet. The electric field-induced reduction in interfacial energy causes the droplet to locally spread out. The resulting change in contact angles sets up a pressure gradient which drives the droplet toward the actuated electrode. This system can also be analyzed from energy-minimization considerations, according to which the droplet minimizes its surface energy by transiting to the actuated electrode. The energy gradient is thus the driving force behind EW-induced motion of a fluid element. Jones [19] compared the contact-angle approach and the energy-based approach and argued that EW-induced motion is primarily an electromechanical phenomenon rather than that resulting from a contact-angle change. An energy gradient-based approach has also been used by Lee *et al* [20] to estimate the EW actuation force on a horizontal fluid capillary The present work further develops and applies the energy gradient concept to develop an analytical model to predict the EW actuation force on a droplet.

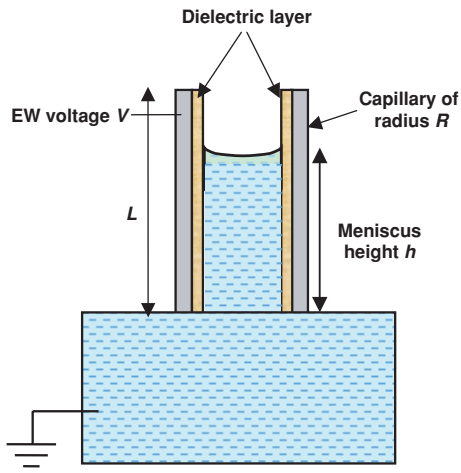

Figure 1. EW-induced capillary rise.

The energy-minimization-based approach is first demonstrated through a prediction of the capillary rise or fall due to an EW voltage applied to the capillary walls; this example serves to highlight the electromechanical nature of EW as emphasized by Jones [19]. Figure 1 shows a circular capillary of radius R and length L with a coating of a dielectric material on its inner wall. The thickness of the dielectric layer is t and its dielectric constant is k. Application of an EW voltage across the dielectric layer changes the capillary height as discussed below. This system can be analyzed by estimating the total system energy as a function of the capillary height h. The total energy is the sum of the dielectric–liquid interfacial energy, the dielectric–air interfacial energy and the potential energy of the liquid column. The system energy when the liquid meniscus is at a height h with an applied voltage V is

$$E(h) = 2\pi Rh\left(\gamma_{\mathrm{SL}}^0 - \frac{k\varepsilon_0 V^2}{2t}\right) + 2\pi R(L-h)\gamma_{\mathrm{SA}}^0 + (\pi R^2 \rho_l h)\left(\frac{gh}{2}\right), \tag{1}$$

where γ_{SL}^0 is the dielectric–liquid interfacial energy in the absence of an EW voltage, γ_{SA}^0 is the dielectric–air interfacial energy, ε_0 is the permittivity of vacuum, g is the acceleration due to gravity and ρ_l is the liquid density. Lippman's [18] equation is used with equation (1) to quantify the decrease in dielectric–liquid interfacial energy upon the application of an EW voltage:

$$\gamma_{\mathrm{SL}} = \gamma_{\mathrm{SL}}^0 - \frac{k\varepsilon_0 V^2}{2t}. \tag{2}$$

The equilibrium height of the meniscus corresponds to the minimum energy position of the system as follows:

$$\frac{\mathrm{d}E(h)}{\mathrm{d}h} = 0 \tag{3}$$

$$h_{\mathrm{eq}} = \frac{2\left(\gamma_{\mathrm{SA}}^0 - \gamma_{\mathrm{SL}}^0\right)}{\rho_l g R} + \frac{k\varepsilon_0 V^2}{t\rho_l g R}. \tag{4}$$

When $\gamma_{\mathrm{SA}}^0 > \gamma_{\mathrm{SL}}^0$, there is a capillary rise even without an EW voltage. Similarly for $\gamma_{\mathrm{SA}}^0 < \gamma_{\mathrm{SL}}^0$, there is a capillary fall in the absence of an EW voltage. Application of an EW voltage

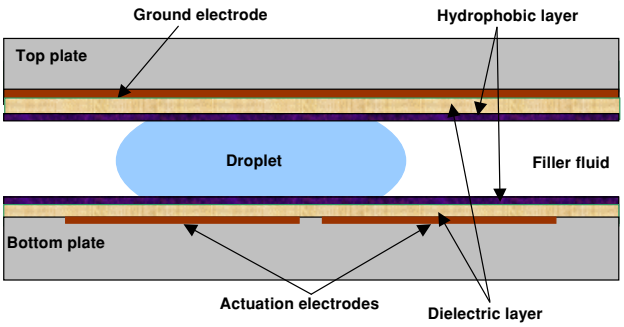

Figure 2. Droplet transport by electrowetting.

decreases the energy required to wet the capillary surface by decreasing γ_{SL} and results in a rise in the meniscus level.

The interfacial energies can be related to the non-EW static droplet contact angle θ_0 by Young's [18] equation,

$$\gamma^0_{SA} - \gamma^0_{SL} = \gamma^0_{LA} \cos\theta_0, \tag{5}$$

where γ^0_{LA} is the liquid–air interfacial energy. Equations (4) and (5) can be combined to yield an expression for capillary rise in terms of the contact angle:

$$h_{eq} = \frac{2\gamma^0_{LA}\cos\theta_0}{\rho_l g R} + \frac{k\varepsilon_0 V^2}{t\rho_l g R}. \tag{6}$$

For the case of no EW voltage, the above equation reduces to the classical estimate for predicting rise and fall of liquids in a circular capillary in terms of the contact angle. There is no reported work on EW-induced capillary rise in circular capillaries; however, Chen and Hsieh [21] used the contact-angle approach to develop an expression for EW-induced capillary rise between flat parallel plates and verified it experimentally. The same expression can also be arrived at by an energy-based analysis of a parallel-plate capillary system, similar to the one carried out for the circular capillary above. Capillarity, with and without EW, can thus be predicted with a knowledge of interfacial energies and areas of the interfaces involved, without invoking the use of contact angles. The above example serves to demonstrate the potential utility of energy-based methods for analyzing EW-based systems.

3. Energy-based modeling of EW actuation force on a droplet

3.1. Physical model

One means for effecting droplet movement [5] using EW is illustrated in figure 2. The device shown consists of two flat plates separated by a selected spacing. Control electrodes are fabricated on the lower plate such that they can be individually addressed. They are covered by a dielectric layer and a thin hydrophobic layer to ensure high initial droplet contact angles. While a hydrophobic layer is not essential to the performance of this device, it allows for larger changes in contact angle upon application of the electric field. The upper plate consists of a single, grounded electrode plane. The top electrode is also coated with a dielectric layer and a hydrophobic layer. The droplet size is chosen to be slightly larger than the electrode pitch so that it overlaps more than one electrode. When a voltage is applied to the electrode on the right of the bottom plate, the dielectric–liquid interfacial tension at the right end of the droplet decreases. The droplet moves toward the energized electrode as a result, and reaches equilibrium when it is at the center of the energized electrode where the surface energy of the droplet is minimized. By pulsing voltages along an array of discrete electrodes, the droplet can be moved continually. It is important to note that the droplet is electrically conducting (e.g., aqueous solution of potassium chloride) and is typically surrounded by a (non-evaporating) filler fluid such as silicone oil [5] so that the droplet evaporation is minimized.

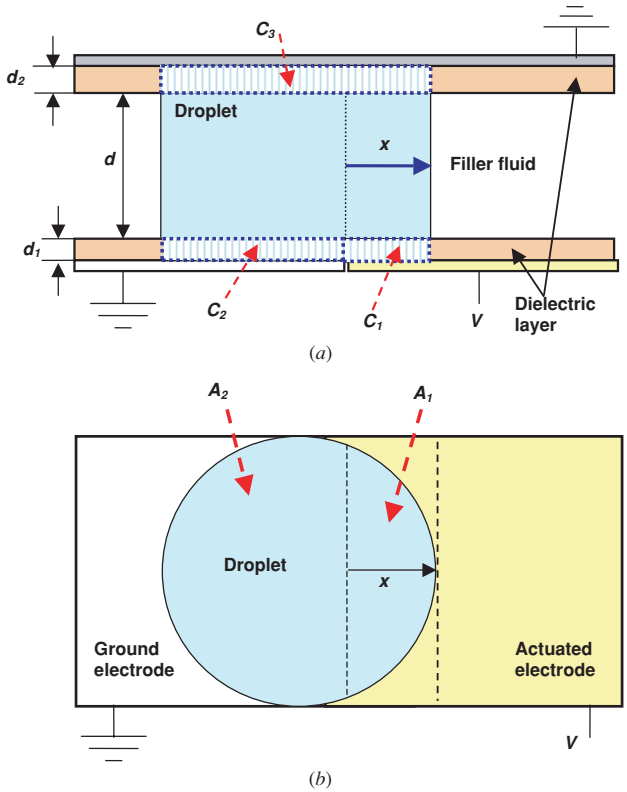

Figure 3. Schematic diagram of a droplet undergoing transition: (*a*) side view and (*b*) top view.

The actuation force on a droplet during the transition can be modeled by analyzing the droplet energy as a function of the droplet position. Figures 3(*a*) and (*b*) show side and top views of an idealized droplet transition, in which the position of the droplet leading edge is tracked by the coordinate x. The droplet is sandwiched between two plates with a separation d as shown in figure 3(*a*) with the electrode width set equal to the droplet diameter. The reduction in interfacial tension is provided by the dielectric layers of thicknesses d_1 and d_2. A voltage V applied to the right electrode on the bottom plate initiates the transition. The left electrode on the bottom plate and the top plate electrode are grounded as in the actuation scheme of Pollack *et al* [5]. The droplet may also be actuated by other voltage distributions or by leaving either the top or the left electrode electrically floating. The proposed modeling framework can be used with any specified voltage actuation scheme to estimate the magnitude of the actuation force and ensure the complete transition to the actuated electrode. The droplet is assumed to move as a rigid body, maintaining its circular shape during the transition. While a stationary

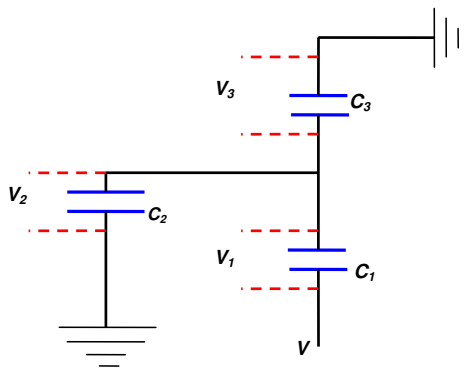

Figure 4. Capacitive network for the estimation of voltages across the dielectric layers.

droplet assumes a circular shape due to symmetry, a droplet in transition could have a distorted ellipse-like shape due to contact-angle hysteresis. It will be shown later that the model can be extended to predict droplet movement for any specified droplet shape during the transition. The total droplet energy consists of the dielectric–liquid interfacial energy γ_{SL} and the droplet–filler fluid interfacial energy γ^0_{LF}. The droplet areas covering the actuated electrode A_1 and the ground electrode A_2 can be estimated from the droplet geometry.

The voltage drops across the dielectric layers causing the reduction of the dielectric–liquid interfacial energy can be obtained from a capacitive network analysis of the system. All the capacitances are represented as parallel-plate capacitors (figure 3(*a*)) which form the capacitive network shown in figure 4. The droplet is assumed to be perfectly conducting so that there is no voltage drop across the droplet. The dielectric in typical EW experiments is much thicker than the ionic double-layer thickness. The dielectric capacitance is thus much smaller than the double-layer capacitance; consequently, the entire voltage drop occurs across the dielectric layer. The electric field lines in all the parallel-plate capacitors are assumed to be perfectly straight and fringing effects at the sides are not accounted for in the present model.

3.2. Analysis

The physical model proposed in the previous section is set into an analytical framework in this section to estimate the actuation force on a circular droplet during the transition. For a droplet of radius r that maintains a circular shape during the entire transition, the areas of the three parallel capacitors are given by

$$A_1(x) = r^2 \cos^{-1}\left(1 - \frac{x}{r}\right) - (r - x)\sqrt{r^2 - (x - r)^2}, \quad (7)$$

$$A_2(x) = \pi r^2 - A_1, \quad (8)$$

$$A_3(x) = \pi r^2. \quad (9)$$

The capacitances of the three parallel-plate capacitors are

$$C_1(x) = \frac{k_1 A_1(x)\varepsilon_0}{d_1}, \quad (10)$$

$$C_2(x) = \frac{k_1 A_2(x)\varepsilon_0}{d_1}, \quad (11)$$

$$C_3(x) = \frac{k_2 A_3(x)\varepsilon_0}{d_2}, \quad (12)$$

where (k_1, d_1) and (k_2, d_2) are the (dielectric constant, thickness) of the lower and upper dielectric layers, respectively (figure 3(*a*)), C_1 is the capacitance of the lower plate dielectric with area A_1, C_2 is the capacitance of the lower plate dielectric with area A_2 and C_3 is the capacitance of the upper plate dielectric (figure 3(*a*)). From the circuit analysis in figure 4, the voltage differences across the three capacitors are

$$V_1(x) = \frac{(C_2 + C_3)V}{(C_1 + C_2 + C_3)}, \quad (13)$$

$$V_2(x) = V_3(x) = \frac{C_1 V}{(C_1 + C_2 + C_3)}. \quad (14)$$

The droplet free energy can now be expressed as the sum of all the interfacial energies:

$$E(x) = \left(\gamma^0_{\mathrm{SL}} - \frac{k_1\varepsilon_0 V_1^2}{2d_1}\right) A_1 + \left(\gamma^0_{\mathrm{SL}} - \frac{k_1\varepsilon_0 V_2^2}{2d_1}\right) A_2 + \left(\gamma^0_{\mathrm{SL}} - \frac{k_2\varepsilon_0 V_3^2}{2d_2}\right) A_3 + \gamma^0_{\mathrm{LF}} A_{\mathrm{side}}. \quad (15)$$

In the above equation, the dielectric–liquid interfacial energy γ^0_{SL} is reduced by the application of an electric field as per Lippman's [18] equation; γ^0_{LF} is the droplet–filler fluid interfacial energy, which remains unchanged; and A_{side} is the cylindrical side area of the droplet, which is assumed to remain constant during the transition. The negative derivative of the energy variation gives the electrical actuation force on the droplet as a function of the transition position x:

$$F(x) = -\frac{\mathrm{d}E(x)}{\mathrm{d}x}. \quad (16)$$

The actuation force has three components corresponding to the three regions of the droplet surface which undergo interfacial energy change under the influence of the applied voltage:

$$F_{\mathrm{act}}(x) = F_1(x) + F_2(x) + F_3(x), \quad (17)$$

where

$$F_1(x) = \frac{k_1\varepsilon_0 V_1^2}{2d_1}\frac{\mathrm{d}A_1}{\mathrm{d}x} + \frac{k_1\varepsilon_0 V_1 A_1}{d_1}\frac{\mathrm{d}V_1}{\mathrm{d}x}, \quad (18)$$

$$F_2(x) = \frac{k_1\varepsilon_0 V_2^2}{2d_1}\frac{\mathrm{d}A_2}{\mathrm{d}x} + \frac{k_1\varepsilon_0 V_2 A_2}{d_1}\frac{\mathrm{d}V_2}{\mathrm{d}x}, \quad (19)$$

$$F_3(x) = \frac{k_2\varepsilon_0 V_3 A_3}{d_2}\frac{\mathrm{d}V_3}{\mathrm{d}x}. \quad (20)$$

$F_1(x)$ and $F_2(x)$ are the force components arising from the dielectric–liquid interfacial energy reduction on the actuated and ground electrodes of the bottom plate, respectively. These forces have contributions from the rates of both area and voltage change of the associated capacitance. $F_3(x)$ has only one contribution originating from the voltage change across the top plate dielectric since the area of C_3 is constant during the transition. It may be noted that this formulation is in terms of area and voltage derivatives, and can thus be extended to any specified shape during the droplet transition, for which the voltage distributions and areas can be computed analytically or numerically. The actuation force results obtained from the present modeling framework are identical to those that would be obtained using a purely electromechanical model consisting of the three capacitances.

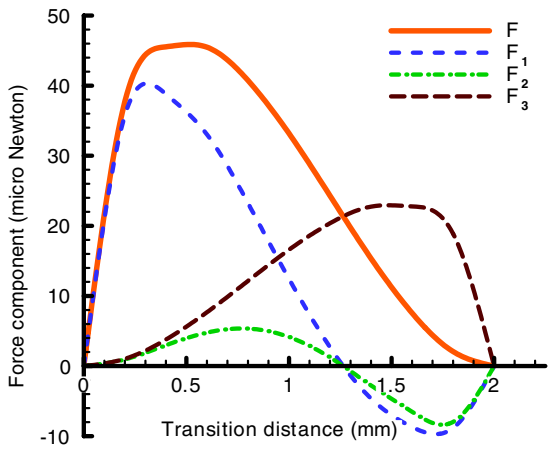

Figure 5. Droplet actuation force during transition.

Table 1. Parameters used for actuation force estimation.

Parameter	Value
Droplet radius (r) = half the electrode width	1 mm
Plate separation (d)	0.3 mm
Dielectric constant: lower plate dielectric (k_1)	3
Dielectric constant: upper plate dielectric (k_2)	3
Thickness: lower plate dielectric (d_1)	1 μm
Thickness: upper plate dielectric (d_2)	1 μm
Actuation voltage (V)	0–50 V

The present model, which commences with the evaluation of surface energy, thus has an electromechanical approach at its core. The electromechanical model can also be used to estimate the actuation force by constructing an energy function involving the equivalent capacitance, which is obtained by lumping together the three capacitances. It is important to note that the results obtained using the present formulation involving the three separate capacitances are identical to those obtained from the equivalent capacitance model.

3.3. Actuation force results

Actuation force results are presented for the droplet transition to an actuated electrode under the conditions outlined in table 1. These parameters are typical of those used for the experimental analysis [5, 16] of EW droplet movement and are used in all subsequent analyses and discussion in this paper unless otherwise indicated.

Figure 5 shows profiles of components of the actuation force as the droplet moves to the actuated electrode. It is seen that the total force is always positive, which ensures the complete transition. The total force is zero at the start of transition and it can be shown from the energy-based analysis that the initial position corresponds to a state of unstable equilibrium (of maximum energy). The position corresponding to the complete transition to the actuated electrode is a stable equilibrium position (of minimum energy), which the droplet eventually attains after overshooting during the first transition and the subsequent oscillatory motion. No experimental measurements of actuation force are available in the literature; thus, actuation force models can only be validated indirectly by using them in a subsequent droplet flow model. Oprins *et al* [16] modeled the EW actuation force on a droplet moving between two plates but with a different actuation scheme; the present results are qualitatively similar to the actuation force results of Oprins *et al* [16].

In terms of the variation of the different actuation force components with the transition distance, F_1 is positive at the start of transition since the first term in equation (18) is dominant during the initial stages because of a large V_1. Conversely, the negative second term of equation (18) representing the gradient of V_1 dominates during the later stages of transition because of an increased C_1. This results in a negative value of F_1 toward the later stages of actuation. A similar explanation can be provided for the behavior of F_2. A net positive force during the later stages of actuation is ensured by F_3 which is positive during the entire transition. Although C_3 is constant during the entire transition, a steady increase in V_3 corresponding to the decrease in V_1 ensures that F_3 stays positive and maintains an overall positive actuation force on the droplet.

3.4. Actuation force dependence on system parameters

The proposed analytical model can be used for estimating the effects of various parameters on the actuation force. First, every component of the actuation force varies as the square of the applied voltage. Next, every component varies directly with the dielectric constant and inversely with the thickness of the dielectric layer. The dielectric layer materials considered in the literature do not vary significantly in their dielectric constant values. Reduction of the dielectric layer thickness is limited by dielectric leakage and breakdown considerations besides the need to avoid chemical reactions (such as electrolysis of droplet solution) which could occur for very thin dielectric layers. Interestingly, the actuation force does not depend on the plate spacing, underscoring the surface origins of this force. Another noteworthy observation is that the actuation force does not depend on the magnitude of dielectric–liquid interfacial tension. This is a direct consequence of Lippman's [18] equation which states that the reduction in the interfacial tension is independent of the absolute value of the interfacial tension. The actuation force is also seen to increase with the droplet radius as a direct consequence of the increased area undergoing the EW-induced interfacial energy change. This increase in force with droplet radius is however directly proportional to the increase in the droplet mass (with the same plate separation) so that the actuation force to droplet mass ratio remains the same. The force prediction model developed can also be used to study the influence on the actuation force of a filler fluid film being present between the droplet and the dielectric. The actuation force in the presence of a filler fluid arises from a reduction in the droplet–filler fluid interfacial tension. The system can then be analyzed by estimating each of C_1, C_2 and C_3 as a series combination of the dielectric capacitance and the filler fluid film capacitance. If the dielectric constants for the filler fluid and the dielectric layer are identical, the effect of the filler fluid is equivalent to an increase in the thickness of the dielectric layer, which leads to a reduction in the actuation force as discussed above.

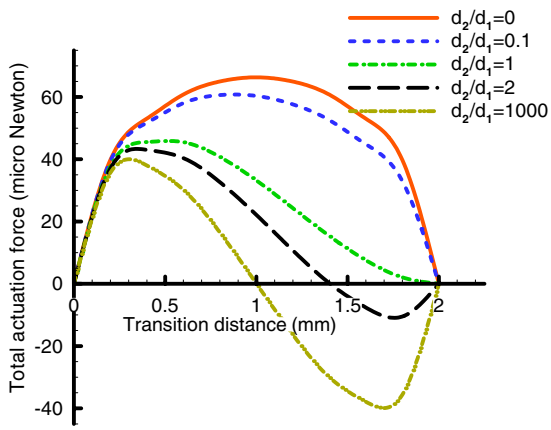

Figure 6. Droplet actuation force dependence on relative thicknesses of the dielectric layers.

In the results presented above, it was assumed that the top and bottom dielectric layer thicknesses were equal. A relative variation of these thicknesses can significantly alter the nature of the actuation force profiles. Figure 6 shows the total actuation force profiles for varying d_2, with d_1 maintained at 1 μm. For $d_2/d_1 > 1$, the total droplet actuation force is not positive throughout actuation, but instead drops to zero at an intermediate position and then becomes negative for the rest of the transition. This result is significant from a design standpoint since a complete transition to the actuated electrode would not occur under these conditions. For very large values of d_2, the actuation force becomes zero at the transition midpoint. This can be explained by observing that C_3 is negligible when compared to C_2 for very large d_2. The capacitive circuit in figure 4 therefore implies that the voltage differences will be determined by C_1 and C_2 alone, and that $C_1 = C_2$, leading to $V_1 = V_2$ at the transition midpoint. The complete symmetry of the situation then implies a zero actuation force at the transition midpoint. Alternatively, this phenomenon of a zero force point during the transition can be understood from a study of the parameters governing the actuation force components. During the later stages of transition, a net positive force is ensured by F_3. With increasing values of d_2, the magnitude of F_3 decreases as compared to the other two components, leading to an overall negative force during the later stages of transition.

The opposite effect is observed for $d_2/d_1 \leqslant 1$ as seen in figure 6, wherein the total actuation force increases for decreasing values of d_2. This can be attributed to F_3 being much larger than the other two components for smaller values of d_2. In the limit of a no top dielectric layer, the actuation force distribution is symmetric with respect to the transition midpoint and the actuation force at every point is maximized, which is desirable for the purpose of reducing actuation voltages. From an application viewpoint, however, a top dielectric layer of finite thickness is necessary to eliminate the possibility of chemical reactions occurring in the droplet solution. EW system design should ensure that the top layer thickness is smaller than that of the bottom layer in order to increase the actuation force [5]. For the ideal case of $d_2 = 0$, the energy-based analysis results in a single-component actuation force:

$$F_{\mathrm{act}}(x) = \frac{k_1 \varepsilon_0 V_1^2}{2d_1} \frac{\mathrm{d}A_1}{\mathrm{d}x}. \tag{21}$$

For subsequent discussions in this paper, the presence and effect of the top dielectric layer are neglected. It is important to note that the presence of a top grounded plate is still essential to the proposed actuation scheme. This ground plane fixes the droplet potential to be equal to the ground potential. In the absence of a top plate, the droplet potential would be decided by the capacitive network. At the transition midpoint, the potential difference across both C_1 and C_2 would then be equal, and the resulting symmetry would lead to a zero actuation force position at the transition midpoint [5], preventing the complete transition to the actuated electrode. Energy-based analyses can be used in this manner to ascertain the feasibility of droplet actuation schemes involving the different electrode configurations and sizes discussed by Pollack *et al* [5].

The results presented above were for a droplet that was circular in shape in plan view. The model can, however, be easily extended for any specified transition droplet shape. All the force components in equation (17) are expressed as derivatives of areas or voltage differences, which can be computed for any specified droplet shape. Four droplet shapes are investigated to explore the significance of droplet shape on the actuation force profile. The droplet shapes include circular, elliptical with different aspect ratios and rectangular with rounded edges, with dimensions as detailed in figure 7. The modeling results of Mohseni and Dolatabadi [7] showed droplets in transition to have steady ellipse-like shapes. Such shapes result as significant contact-angle hysteresis or contact-line friction causes the droplet to depart from its circular shape. Rectangular shapes with rounded edges could be obtained by setting the droplet volume equal to the volume required to cover a complete rectangular electrode. In this case, the droplet would assume the shape of the electrode to minimize its

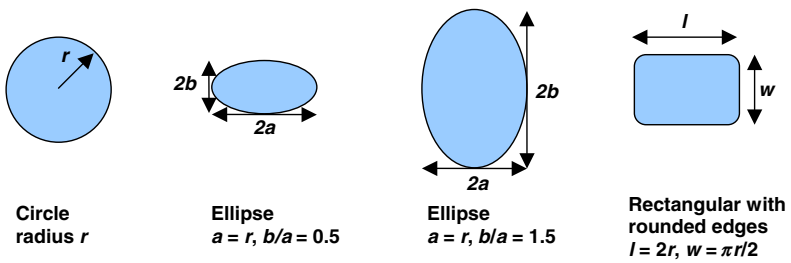

Figure 7. Droplet shapes studied for actuation force variation.

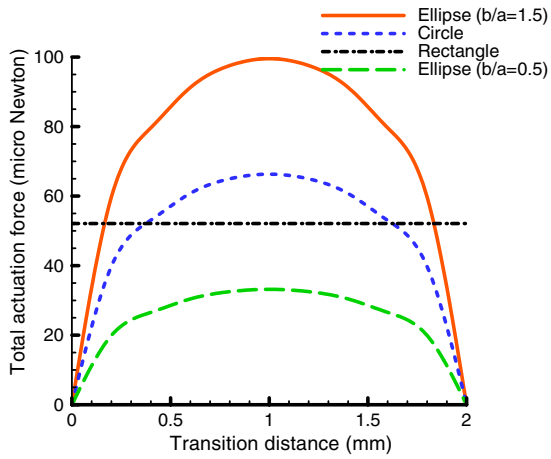

Figure 8. Actuation force profiles for various droplet shapes.

surface energy in preference to a circular shape. The transition distance (equal to electrode width) and plate separation are maintained equal for all the droplets. The width of the rectangular droplet is adjusted to make the droplet mass equal to that of the circular one. Such an adjustment is, however, not possible for the elliptical droplets since the droplet transition lengths are kept same for both shapes; the two elliptical droplets thus have different masses from the circular droplet corresponding to different widths of the elliptical droplets.

Figure 8 compares the actuation force profiles for the four droplets under the condition of an absent top dielectric layer. The actuation force is highest for the elliptical droplet with $b/a = 1.5$ and lowest for the elliptical droplet with $b/a = 0.5$. It should be noted that these droplet sizes correspond to the largest and smallest (in terms of mass) droplets, respectively. The variation of the actuation force normalized with the droplet mass is identical for the circular and the two elliptical droplets. The actuation force is constant for the rectangular droplet as a result of the constant droplet width. This analysis serves to illustrate the versatility of the present modeling approach in terms of its capability to analyze complex features of EW droplet motion.

4. Modeling EW-induced droplet motion

4.1. Model description

An accurate prediction of EW-induced droplet motion depends on a realistic estimation of the EW actuation force and the forces opposing droplet motion. The opposing forces of significance are the shear force due to the top and bottom plates, the viscous force exerted by the filler fluid and the contact-line friction force. Additionally, a threshold EW voltage [17] is required to initiate droplet movement by overcoming contact-angle hysteresis. The nature and dynamics of several of these opposing forces is not well understood, which renders difficult the development of a model which takes these forces into account. These phenomena have therefore been handled with semi-empirical models in the literature. The shear stress from the top and bottom plates has been modeled under the assumption of a velocity profile in the droplet [8, 16]. While this provides an approximate estimate for the wall shear, the assumption of a timewise constant velocity profile in a discrete moving droplet is incorrect. However, no flow visualizations or experimental measurements inside these moving droplets have been reported.

Contact-line friction is another phenomenon which is difficult to model. Contact-line friction originates from intermolecular attraction forces near the contact line and the nature and magnitude of this force and its relation to surface roughness is poorly understood. Oprins *et al* [16] related the contact-line friction to experimentally measured droplet hysteresis angles, but this approach is of limited use since droplet hysteresis is extremely difficult to predict and depends on the fluid and solid properties in addition to the surface texture. Schneemilch *et al* [22] investigated the dynamics of a moving contact line in the presence of an external electric field and compared it to a molecular-kinetics model for contact-line motion. The model matched experiments reasonably well, but the model was based on certain molecular parameters and empirical constants which are not available for all materials and have not been directly related to measurable physical properties such as surface tension and viscosity. Also, the model dealt with the influence of an electric field on an already moving contact line, and not with field-induced contact-line motion. A commonly used modeling approach based on the molecular interaction theory of Blake [15] consists of estimating contact-line friction as being proportional to a power of the contact-line velocity. Ren *et al* [17] and Chen *et al* [21] assumed a linear relationship between the contact-line friction and contact-line velocity and obtained the proportionality constant from a comparison of experimental and modeling results.

The present work is not aimed at resolving these challenges to droplet motion prediction. Instead, the objective is to study the influence of each of the opposing forces on overall droplet motion and identify those dominant forces and parameters which need to be explored in greater detail. The droplet transport situations considered here are those where the finer details of fluid motion (and the associated complex modeling) are not required. The droplet is considered as a single discrete mass moving through the filler fluid as a result of an EW actuation force, with all the opposing forces represented by simplified algebraic expressions.

The plate shear stress is modeled in a similar manner as in previous approaches by the assumption of a velocity profile in the droplet with zero slip boundary conditions at the top and bottom walls. A conservative estimate for the shear stress is arrived at by assuming a parabolic velocity profile which leads to a higher shear stress than that obtained from a linear velocity profile for the same average velocity. The total shear force exerted by the top and bottom walls is then obtained as

$$F_w = \left(\frac{6\mu_l v}{d}\right)(2\pi r^2), \tag{22}$$

where v is the droplet velocity and μ_l is the droplet viscosity. The viscous shear due to the filler fluid is estimated by considering the droplet as a rigid body moving through the filler fluid and using the correlation for the viscous drag on a cylinder in a cross flow:

$$F_f = \left(\tfrac{1}{2}C\rho_f v^2\right)(2rd), \tag{23}$$

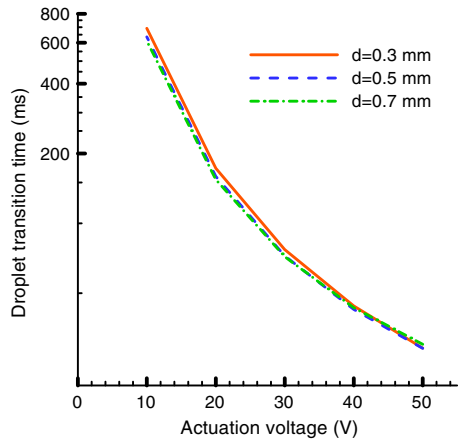

Figure 9. Droplet transition time dependence on voltage and plate spacing (transition distance is 2 mm).

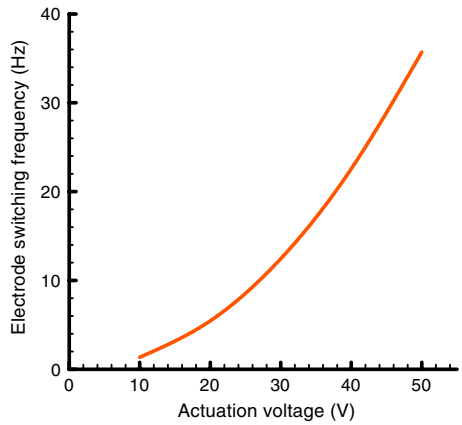

Figure 10. Electrode switching frequencies needed to ensure continuous motion of a 1 mm radius droplet over an array of electrodes.

where C is the drag coefficient for a cylinder in a cross flow and ρ_f is the filler fluid density. The contact-line friction force is estimated using the approach of Ren *et al* [17] where the friction force is assumed proportional to the droplet velocity:

$$F_{\mathrm{cl}} = (\zeta v)(4\pi r), \tag{24}$$

where ζ is a proportionality coefficient. From the above equations, it is seen that all the opposing forces are related to the droplet velocity. The overall equation governing EW-induced droplet motion is then written as

$$m\frac{\mathrm{d}^2 x}{\mathrm{d}t^2} = F_{\mathrm{act}} - F_{\mathrm{w}} - F_{\mathrm{f}} - F_{\mathrm{cl}}, \tag{25}$$

where m is the droplet mass.

4.2. Droplet motion results

The above differential equation was solved using MATHEMATICA[1] to obtain the droplet position and velocity variation with time. The simulations were carried out for a circular droplet moving to the actuated electrode in the absence of a top plate dielectric. The droplet properties were taken to be those of water, while the filler fluid was assumed to be silicone oil. The coefficient ζ needed for contact-line friction force estimation was assumed [17] to be $\zeta = 0.04$ N s m^{-2}. From the actuation force plots in figure 6, it is observed that the electrical actuation force is zero at the initial rest position of the droplet. The droplet movement was therefore initiated from rest in the model by displacing the droplet by 1% of the total transition distance, thereby ensuring the presence of a non-zero actuation force to start droplet motion.

Figure 9 shows the transition time required for a 1 mm radius droplet to move to the actuated electrode as a function of the applied voltage for three plate spacings. The droplet has a finite velocity when it completes the transition. Subsequent droplet motion is determined by the voltage of the electrode adjacent to the actuated electrode in the direction of the droplet velocity. When this adjacent electrode is grounded, the droplet oscillates about the center of the actuated electrode before coming to rest, owing to viscous and contact-line friction-induced damping. Under actual experimental conditions, this oscillatory behavior would be difficult to demonstrate, since contact-angle hysteresis is not accounted for in the model. From figure 9, it is seen that droplet transition times strongly depend on the actuation voltage, which underscores the dominant influence of the voltage on the actuation force. No significant dependence of the transition time on the gap spacing is seen, except in the low-voltage, low-velocity regime where a slight decrease in the transition time is observed with the increased gap spacing. While an increase in the gap spacing leads to an increased droplet mass, the opposing viscous forces also change with gap spacing. The net effect is the absence of any substantial dependence of the transition time on the gap spacing. Average and peak velocities of 7 cm s^{-1} and 10 cm s^{-1} respectively were obtained for an actuation voltage of 50 V, which are comparable to the experimental results of Pollack *et al* [5] and the modeling results of Oprins *et al* [16].

The model can also be used to study continuous droplet transport over an array of sequentially excited electrodes. In this case, the initial droplet position corresponds to the zero actuation force position, with a finite initial velocity imparted to the droplet. This velocity is determined by applying periodic velocity boundary conditions at the beginning and end of transition. The required transition time so obtained can be used to estimate the electrode switching frequencies needed to sustain a continuous droplet motion. Figure 10 shows the electrode transition frequencies for a 1 mm radius droplet as a function of the applied voltage. The switching frequencies increase with increasing voltage as a result of faster transitions.

Droplet radius is an easily controlled parameter and its impact on droplet motion was also investigated. The droplet transition time decreases with a smaller droplet radius, but this is primarily the consequence of a reduced transition distance (which is equal to the droplet diameter). A change in the droplet radius changes the actuation force and the droplet mass by the same proportion; consequently, the transition velocities do not vary significantly. In the present results, the peak droplet velocity increased from 9.15 cm s^{-1} to 10.85 cm s^{-1} corresponding to a decrease in the droplet radius from 1.5 mm to 0.5 mm at 50 V. The droplet velocity is a key parameter which determines the rate of microfluidic operations in lab-on-chip devices, and the present results show that scaling

[1] MATHEMATICA 5 Reference manual 2005, Wolfram Research Inc.

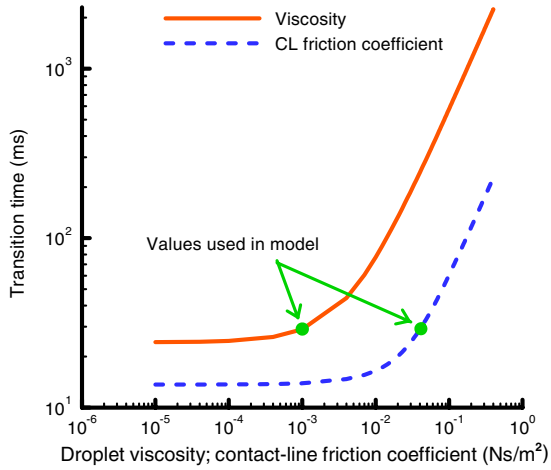

Figure 11. Transition time dependence on contact-line friction coefficient and droplet viscosity.

down droplet sizes alone does not yield significantly higher velocities. The actuation voltage plays a much more dominant role in influencing the droplet actuation force and thus the droplet velocity.

The opposing forces in the present analysis were modeled using semi-empirical expressions involving fluid properties and the contact-line friction coefficient. The sensitivity of the model results to the values assigned to two such variables is explored next. The effect of varying the contact-line friction coefficient ζ and droplet viscosity μ_l on the droplet transition time is examined in figure 11. The two curves in figure 11 correspond to changing the values of ζ and μ_l, with all other parameters being fixed. The slope of the curve corresponding to varying values of ζ shows that the model is sensitive to the value of ζ around the value $\zeta = 0.04$ N s m^{-2}, which has been used in the present work. This underlines the need for using accurate values of ζ to obtain reliable results. The sensitivity to droplet viscosity variation is small near the value of $\mu_l = 0.001$ N s m^{-2} for a water droplet. Since droplet viscosity is a measure of the wall shear stress, it follows that wall shear is not a dominant force for the droplet movement situation considered here. Another significant ramification of the results in this figure concerns the influence of temperature on droplet movement. The decrease in droplet viscosity with temperature should by itself not affect droplet motion significantly since the lower viscosity will fall in the viscosity-insensitive regime of the model parameter space. Droplet dynamics is thus governed predominantly by contact-line friction rather than by viscous forces for the situation modeled in this work, which agrees with the observations of Ren *et al* [17]. Parametric analyses of this kind are useful in estimating the relative strength of various opposing forces and highlighting phenomena which need more reliable and accurate modeling.

5. Conclusions

An energy-based analysis methodology is developed in this work for modeling electrowetting-based systems. The use and advantages of this analysis approach are demonstrated for performance estimation of such electrowetting-based systems. Analyses based on minimization of system energy can be used to predict overall performance, while circumventing the difficulties in representing the full complexity of all the physical phenomena involved. The origin and the fundamental physics behind EW droplet actuation are explored in detail and extensive parametric variation is employed to arrive at conditions which maximize the EW actuation force. The versatility and convenience of the energy-based model are demonstrated by employing the model to analyze various aspects of the actuation force estimation, including the conditions required to ensure a continuous positive actuation force and the influence of droplet shapes.

The actuation force model is then combined with semi-empirical models for predicting forces opposing droplet motion to yield a simplified model for predicting droplet motion under EW actuation. Various aspects of droplet motion are discussed and parametric variation employed to study the significance of droplet geometry, droplet viscosity and contact-line friction coefficient on droplet motion. It is seen that contact-line friction is a dominant phenomenon for the EW-induced droplet movement situations considered in the available literature. Reliable prediction of droplet motion thus depends on the use of models which ensure accurate prediction of contact-line friction. Likewise, contact-angle hysteresis needs to be accounted for to predict droplet motion in a more realistic manner.

References

[1] Kim C J 2001 Micropumping by electrowetting *ASME Int. Mech. Eng. Cong. and Expo. (New York)* IMECE2001/HTD-24200

[2] Sammarco T S and Burns M A 1999 Thermocapillary pumping of discrete drops in microfabricated analysis devices *AIChE J.* **45** 350–66

[3] Chiou P Y, Moon H, Toshiyoshi H, Kim C J and Wu M C 2003 Light actuation of liquid by optoelectrowetting *Sensors Actuators* A **104** 222–8

[4] Geng X, Yuan H, Oguz H N and Prosperetti A 2001 Bubble-based micropump for electrically conducting liquids *J. Micromech. Microeng.* **11** 270–6

[5] Pollack M G, Shenderov A D and Fair R B 2002 Electrowetting-based actuation of droplets for integrated microfluidics *Lab on a Chip* **2** 96–101

[6] Pollack M G and Fair R B 2000 Electrowetting-based actuation of liquid droplets for microfluidic applications *Appl. Phys. Lett.* **77** 1725–6

[7] Mohseni K and Dolatabadi A 2005 Electrowetting droplet actuation in micro scale devices *43rd AIAA Aerospace Sci. Mtg. and Exhibit (Nevada)* AIAA-677

[8] Kuo J S, Spicar-Mihalic P, Rodriguez I and Chiu D T 2003 Electrowetting-induced droplet movement in an immiscible medium *Langmuir* **19** 250–5

[9] Yi U C and Kim C J 2005 EWOD actuation with electrode-free cover plate *13th Int. Conf. on Solid-State Sensors, Actuators and Microsystems Seoul (South Korea)*

[10] Torkkeli A, Saarilahti J, Haara A, Harma H, Soukka T and Tolonen P 2001 Electrostatic transportation of water droplets on superhydrophobic surfaces *14th Int. IEEE Conf. on MEMS* pp 475–8

[11] Paik P, Pamula V K and Chakrabarty K 2005 Adaptive hot-spot cooling of integrated circuits using digital microfluidics *Proc. IMECE 2005 (FL, USA)* IMECE2005-81081

[12] Fair R B, Srinivasan V, Ren H, Paik P, Pamula V K and Pollack M G 2003 Electrowetting-based on-chip sample

processing for integrated microfluidics *IEEE Inter. Electron Devices Meeting*

[13] Quilliet C and Berge B 2001 Electrowetting: a recent outbreak *Curr. Opin. Colloid Interface Sci.* **6** 34–9

[14] Quinn A, Sedev R and Ralston J 2003 Influence of the electrical double layer in electrowetting *J. Phys. Chem.* B **107** 1163–9

[15] Blake T D 1993 Dynamic contact angles and wetting kinetics *Wettability, Surfactant Science Series* vol 49 (New York: Dekker) pp 251–309

[16] Oprins H, Vandevelde B, Beyne E, Borghs G and Baelmans M 2004 Selective cooling of microelectronics using electrostatic actuated liquid droplets-modeling and experiments *Int. Workshop on Thermal Investigations of ICs and Systems (Cote d'Azur, France)* pp 207–12

[17] Ren H, Fair R B, Pollack M G and Shaughnessy E J 2002 Dynamics of electro-wetting droplet transport *Sensors Actuators* B **87** 201–6

[18] Mugele F and Baret J C 2005 Electrowetting: from basics to applications *J. Phys.: Condens. Matter* **17** R705–74

[19] Jones T B 2005 An electromechanical interpretation of electrowetting *J. Micromech. Microeng.* **15** 1184–7

[20] Lee L, Moon H, Fowler B, Schoellhammer T and Kim C J 2002 Electrowetting and electrowetting-on-dielectric for microscale liquid handling *Sensors Actuators* A **95** 259–68

[21] Chen J H and Hsieh W H 2006 Electrowetting-induced capillary flow in a parallel-plate channel *J. Colloid Interface Sci.* **296** 276–83

[22] Schneemilch M, Welters W J J, Hayes R A and Ralston J 2000 Electrically induced changes in dynamic wettability *Langmuir* **16** 2924–7